Microstructure, texture and mechanical properties with raw surface states of Ti-6Al-4V parts built by L-PBF

Quentin Gaillard, Sophie Cazottes, X Boulnat, Sylvain Dancette, Christophe Desrayaud

HAL Id: emse-04129436

https://hal-emse.ccsd.cnrs.fr/emse-04129436v1

Submitted on 15 Jun 2023

6th CIRP Conference on Surface Integrity

Microstructure, texture and mechanical properties with raw surface states of Ti-6Al-4V parts built by L-PBF

Quentin Gaillard[a,b,*], Sophie Cazottes[b], Xavier Boulnat[b], Sylvain Dancette[b], Christophe Desrayaud[a]

[a]*Mines Saint-Étienne, Université de Lyon, LGF, UMR CNRS 5307, F-42023 Saint-Étienne, France*
[b] *INSA Lyon, Université de Lyon, MATEIS, UMR CNRS 5510, F-69621 Villeurbanne, France*

* Corresponding author. Tel.: +33-477-426-631; *E-mail address:* quentin.gaillard@emse.fr

Abstract

Due to dramatic thermal gradients and cooling rates induced by Laser Powder Bed Fusion (L-PBF), Ti-6Al-4V as-built parts show a fine martensitic microstructure with high residual stresses that are detrimental for their mechanical behaviour. In order to optimize the properties and meet the product requirements, post-processing heat treatments are often compulsory. The present work first describes the microstructure (residual stresses, beta grains and laths size, crystallographic texture) and the mechanical behaviour (impact and tensile tests) of as-built parts with raw surface. Then, one discusses the effect of a stress-relieve sub-transus heat treatment on the strength/ductility compromise.

Keywords: Laser powder bed fusion ; Ti-6Al-4V ; microstructure ; mechanical properties ; heat treatments

1. Introduction

For some years now, additive manufacturing (AM) of metallic components allows creating strong, functional and fully dense metallic parts. Among all the existing processes, Laser Powder Bed Fusion process (L-PBF) has the ability to create medium size parts of high geometrical complexity with a good precision. The process is described in many existing works and the reader is referred to Ref. [1] for more details. To ensure optimal building conditions (i.e. to maximize the density and to limit the number of defects and their criticality), the influence of different process parameters such as laser power, scan speed, scan strategy, layer thickness etc. have been investigated extensively [2,3,4]. Consequently, this process henceforth shows a good efficiency for building many materials and especially titanium alloys.

Ti-6Al-4V (TA6V) is the most widespread commercial titanium alloy, which is often employed in the aerospace and biomedical sectors. TA6V is a α + β titanium alloy because α and β microstructural phases coexist at the equilibrium at room temperature. This feature enables to obtain a good combination of strength and ductility when the thermo-mechanical manufacturing cycle of the material is well defined. As shown in previous studies, the high thermal gradients and cooling rates involved during melting of powder particles lead to a microstructure consisting of a fine acicular martensitic needle-like phase called α′ [5,6,7]. Another microstructural issue for L-PBF TA6V is the presence of columnar prior β grains, elongated in the building direction and whose height can span several millimeters [4,8].

In addition, as a consequence of the high thermal gradients, large Residual Stresses (RS) progressively appear in the part as layers are built during the process [9]. These RS are particularly detrimental for the mechanical behavior and the fatigue performance of the material [10] as they present a macroscopic state consisting of tensile RS near the surface, balanced by compressive RS in the center [11,12,13,14]. The presence of RS in the parts also limit their dimensional precision.

Typical tensile strength properties of the L-PBF TA6V parts are both a high yield stress and ultimate tensile strength but a

poor ductility, with an elongation at break lower than 10% in the majority of the reported results [8,15,16,17,18]. To obtain a variety of required mechanical properties for particular applications, the ductility of TA6V products fabricated by L-PBF has to be improved. Although it has been reported that the ductility is mainly controlled by the presence of defects such as pores or lacks of fusion in the parts [2,19], but also by the surface state [20], it seems that the presence of a fine microstructure and large RS are placed among the main issues that lead to the poor elongation at break in the as-built fully dense parts. Thus, by designing suitable post-production heat treatments, it is possible to improve the mechanical behavior by achieving both microstructural evolutions that helps to balance strength and ductility, and reductions of the RS that have been built up during the L-PBF process [19,21]. Nowadays, this topic is of main interest for industrial applications and a lot of research are currently performed on it because the economic feasibility of manufacturing TA6V parts by L-PBF primarily depends on the cost of the post-treatments required [22]. Furthermore, most of the published studies only focus on the relations between heat treatments, microstructure and properties without taking into account the surface state of the samples tested (they are most of the time machined into coupons) or the orientation of the samples in relation to the building direction (named Z in this study).

Hence, while displaying the effects of a post-processing heat treatment, this paper aims at detailing the as-built characteristics (microstructure, texture, RS) and the mechanical properties (impact and tensile test properties) of L-PBF TA6V extensively.

2. Materials and methods

In the present work, a commercial spherical plasma atomized TA6V powder with a size distribution ranging from 5 µm to 25 µm was used. The chemical composition (weight. %) of the batch of grade 5 TA6V powder is detailed in Table 1.

Table 1. Chemical composition of the TA6V powder used in this study.

Element	Ti	Al	V	Fe	O	C	N	H
$w\%_{min}$	Rest	5.50	3.50	-	-	-	-	-
$w\%_{max}$	Rest	6.50	4.50	0.25	0.18	0.08	0.05	0.015

The samples were built near-net shape using a FormUp 350 L-PBF equipment. The machine is equipped with two YAG fibre lasers, which possesses a maximum laser power of 500 W and a laser spot size of 70 µm. The building process was performed in an argon protective atmosphere with an oxygen concentration measured around 500 ppm in the chamber. No preheating of the base plates was performed. A meander scanning pattern was applied with the scanning direction rotated by 90° after each layer deposition.
In accordance with the ISO/ASTM 52900 standard, the orientations of the parts are described in this research using the axis of the L-PBF machine that are parallel to the longest and second longest dimensions of the parts. As shown in Fig. 1, four

vertical ZX / ZY, four horizontal XZ / YZ and four flat XY / YX dog-bone shape tensile specimens were built on two 174x174 mm² plates in a single batch. These tensile bars were built with a gauge length, width and thickness of 35 mm, 7 mm and 3 mm respectively. In addition, 20 Charpy impact V-notch vertical specimens (named ZX / ZY / Z-X / Z-Y) were built to study the resilience of the material. Finally, two $15 \times 15 \times 15$ mm³ cubes, two single arm cantilevers and a $40 \times 30 \times 70$ mm³ block were built to study the microstructure and the RS. After building, the samples were separated from the base plates by wire electrical discharge machining (EDM).
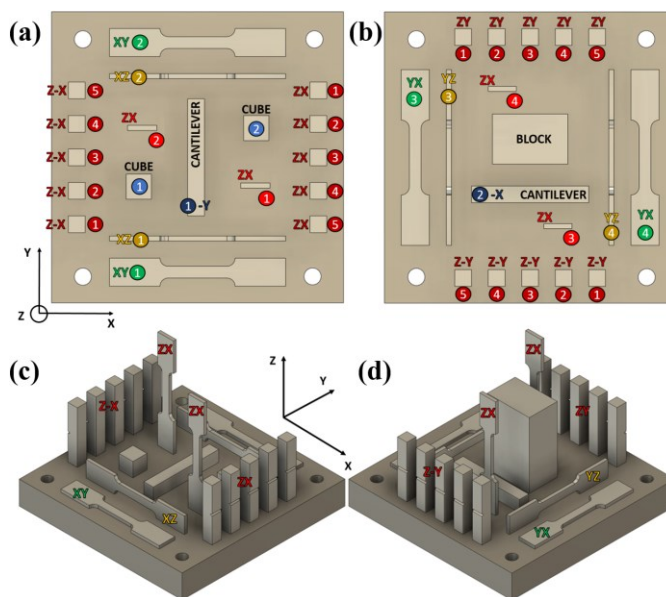

Fig. 1. (a) Left plate, (b) right plate top views and (c) left plate, (d) right plate side views models of the specimens built in this research. The tensile bars were built in three orientations referred to as ZX / ZY, XZ / YZ and XY / YX.

Two batches of the plates introduced in Fig. 1 were fabricated. The first batch underwent no post-processing treatment; it will be referred as the "as-built" condition. However, before cutting the parts, the plates of the second batch were heat treated at 720°C for 2h under secondary vacuum better than 5×10^{-4} mbar. Once the treatment was achieved, furnace cooling ($2 - 3°C/min$) was applied by turning the heating off then argon quenching occurred when the temperature was below 400°C. It will be referred as the "stress-relieved" condition.

No surface finish was made on none of the samples and each of them were tested with raw surface states. The surface roughness was measured using a confocal profilometer equipped with a nano point scanner (NPS) system.

The tensile tests were performed at room temperature with an Instron Model 1186 tensile system equipped with a strain gauge extensometer. The tests were conducted at a cross-heat displacement rate of 0.525 mm/min. Yield stress, ultimate tensile stress and elongation to failure were determined according to the NF EN ISO 6892-1 standard.

X-Ray diffraction measurements of the RS in the as-built state were realised on the block with an MRX X-Raybot using

the $\sin^2(\psi)$ method following the NF EN 15305 standard [23]. The diffractometer was equipped with a Cu K$_\alpha$ ($\lambda = 1.54$ Å) X-Ray tube source operating at 20 kV and a Ni K$_\beta$ filter. The peak shifts that correspond to lattice strain in the diffraction peak position at 2θ of 142° ({213} plane of the α phase of Ti) was measured using 13 values of ψ angle between −45° and +45°. In addition, to evaluate the evolution of RS between the as-built and the stress-relieved conditions, cantilevers deflexion was measured.

Examinations of the microstructure were made on the cubes after grinding and polishing with SiC paper up to 320 grit size followed by 9 μm diamond solution and chemical-mechanical polishing with a mixture of colloidal silica, hydrogen peroxide and ammonia. Before performing Electron Backscattered Diffraction (EBSD), a vibratory polishing step with colloidal silica occurred. After etching for 90s with Kroll reagent, micrographs of the samples were performed on an Olympus GX51 equipped with a motorized stage. EBSD maps were recorded on a ZEISS Supra 55VP SEM equipped with an Oxford Instrument Symmetry camera, operating at 20 kV.

3. Results and discussion

3.1. Surface roughness

The surface roughness of the block and of the tensile bars measured with a confocal system on various planes is presented in Table 2. The results provided are the average values and standard deviation of the arithmetic mean deviation calculated from 6 surface profiles made on each plane.

Overall, the surface roughness measured on the samples is rather low compared to other as-built roughness parameters given for the same material built by L-PBF [8,24]. This is explained by the small granulometry of the powder used in this fabrication but also by a sample contour forming strategy occurring during the process.

Table 2. Surface roughness of the L-PBF samples with no surface finishing.

Surface roughness R_a (μm)	
Block – XY top surface	5.19 ± 0.46
Block – XY bottom surface	3.46 ± 0.10
Block – XZ/YZ lateral surfaces	6.02 ± 0.42
XY/YX tensile bars – XY top surface	3.55 ± 0.31
XY/YX tensile bars – XY bottom surface	3.28 ± 0.03
XZ/YZ tensile bars – XZ/YZ lateral surfaces	5.16 ± 0.51
XZ/YZ tensile bars – XY bottom surfaces	0.62 ± 0.20
ZX tensile bars – XZ/YZ lateral surfaces	5.32 ± 0.44

Furthermore, it can be noticed that the roughness of the bottom surfaces is lower because they are generated after removing the samples from the base plate by wire EDM. It applies to all bottom surfaces except for the XY bottom surface of the XZ / YZ tensile bars which is machined to remove the support structures, explaining the significant drop in surface roughness measured.

3.2. Residual stresses

RS X-Ray diffraction measurements made in the middle of the planes of some as-built samples after removal from the base plate are listed in Table 3. The angle between a fixed direction in a plane of the block and the projection in that plane of the normal of the diffracting plane was taken equal to zero in order to measure the principal stresses in the sample's axis system. It was not possible to measure a value for the XY bottom surface because of the formation of a colorful titanium oxide thin film in the heat affected zone during cutting by wire EDM.

The results show that high tensile RS are formed at the surface of the as-built L-PBF TA6V components which is consistent with other results reported in the literature with an optimized scan strategy to build fully dense parts with no heating of the building platform [8,11,16]. It is also noticeable that the RS measured on the Charpy impact sample are lower than the ones measured on the block. The higher tensile RS of the block are certainly inherited from its huge dimensions, illustrating the fact that the RS levels are influenced by the height (number of layers) and by the thickness of the samples [9].

While doing the measurements on the as-built surfaces of the block, it was difficult to get a sufficient signal for the {213} plane's peak and therefore the uncertainty calculated with the $\sin^2(\psi)$ method is important. This lack of signal can be directly attributed to the surface roughness of the part as it is estimated that the X-Ray penetration depth in titanium with a Cu source does not exceed 6 μm when the tilting angle ψ is zero [23]. Thus, the RS measurements presented in Table 3 were acquired in the rough layer of the material. To measure the RS near the surface and enhance the quality of the measurements, a possibility would be to perform electro-polishing to remove this rough layer without adding mechanically induced stresses in the material. Electro-polishing could be also carried out to determine the variation of RS as a function of the depth from the surface by performing successive material removal followed by successive stress analyses [23].

Table 3. Residual stress analysis on the as-built L-PBF TA6V samples.

Principal stresses measured in the middle of the planes (MPa)		
Block – XY top surface	σ_X	559 ± 100
Block – XY bottom surface	σ_X	/
Block – XZ lateral surface	σ_Z	566 ± 79
Block – YZ lateral surface	σ_Z	689 ± 83
Charpy ZY$_1$ – XY top surface	σ_X	201 ± 62
Charpy ZY$_1$ – ZX lateral surface	σ_Z	405 ± 74

From fig. 2, it is clear that approximately all the RS of the as-built components are eliminated by the stress-relief heat treatment. It was in fact not possible to measure any stresses in the stress-relieved samples by X-Ray diffraction as the uncertainties of measurement because of the surface roughness are much higher than the stresses themselves.
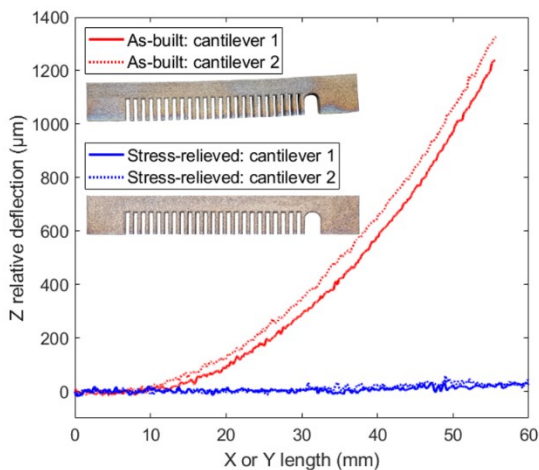
Fig. 2. Deflection of the as-built and stress-relieved cantilevers after removal from the base plate measured using confocal profilometry.
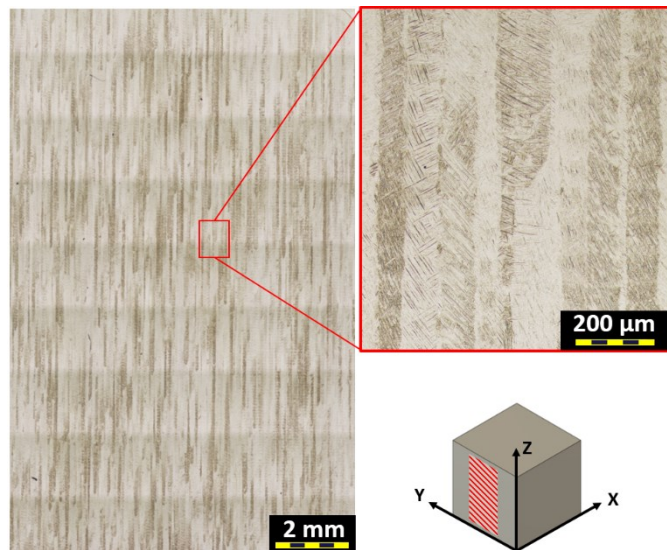
No cracks, delamination or deformation of any of the stress-relieved samples was noticed. In contrast, without the stress-relieved treatment, bending of the as-built XY/YX and XZ/YZ tensile bars as well as cracks at the bottom of the as-built block happened after removal from the base plate.

3.3. Microstructure and crystallographic texture

Fig. 3 shows a side YZ plane view of an as-built cube after polishing and chemical attack, revealing the long columnar prior β grains, morphologically oriented parallel to the building direction. This columnar shape is formed because of the thermal gradients and extremely high cooling rates from the liquid phase to the β domain ($10^6 - 10^7$ K/s according to Ref. [6]). The β phase growth is epitaxial across the deposited layer and is driven by thermal gradients along the building direction. In fact, at every crossing of the laser beam part of the columnar

Fig. 3. Optical micrographs showing the columnar parent β grains in the YZ lateral plane of an as-built TA6V cube built by L-PBF.

grains in the already formed layer are remelted. Then, the new β phase formed during solidification grows epitaxially to the β phase below, leading to this strongly morphologically textured grains [17]. The average width of these grains, estimated with the ImageJ software, is $64,2 \pm 6$ μm which is really close to the hatch spacing, as reported by several other authors [18,19,21].

Inside the prior β grains, a very fine microstructure consisting of acicular α′ martensite can be observed. The α′ needles are very thin due to the very fast cooling rates from the β domain, approximately 10^4 K/s from ref. [17]. This fine microstructure is better visible in Fig. 4.a, which shows a backscattered electron (BSE) image taken in the YZ plane of an as-built cube. According to the definitions and model proposed by Yang et al. [8], the martensitic transformation upon cooling
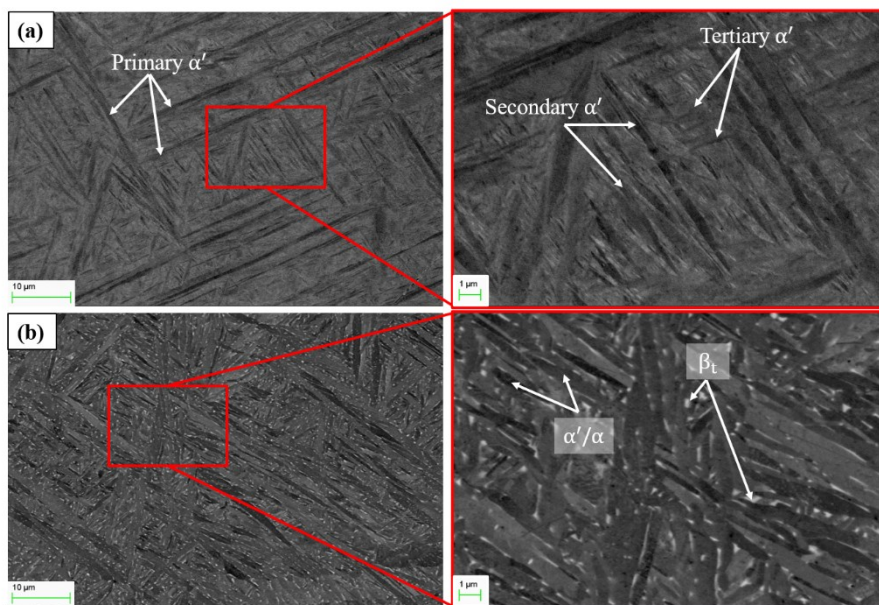

Fig. 4. Backscattered electron pictures showing the microstructure in the YZ lateral plane of an as-built (a) and a stress-relieved (b) TA6V cube built by L-PBF.

leads to a hierarchical structure presenting various α′ needles sizes denoted as primary, secondary, tertiary and quartic α′. The resolution of the BSE mode with the acquisition parameters used was not sufficient to see the quartic needles as their thickness is estimated to be around 10 nm [6,25]. Due to their small size, tertiary and quartic α′ needles represent a low volume fraction in the microstructure in comparison to primary and secondary α′ needles. The average thickness of the two latter was estimated around 0.45 μm in this study by applying grain reconstruction methods from EBSD data.

During the stress-relieve sub-transus heat treatment the phase transformation $α′ → α + β_t$ take place and the microstructure consist of a mixture of α/α′ with a small portion of transformed β from the decomposition of the martensite (Fig. 4.b). The estimated volume fraction of $β_t$ was estimated around 2.7 ± 0.3 % by image analysis of 10 XY and 10 YZ BSE pictures. This result is consistent with other reported values for similar stress-relieve heat treatments performed [5,17]. It can be observed from Fig. 4.b that the tertiary and quartic α′ of the as-built state are not visible anymore. However, the estimated average thickness of the biggest α/α′ laths is 0.49 μm, close to the value measured for the as-built condition. From this observation it can be concluded that the stress-relieve treatment seems not to affect the biggest α′ structures but conduct to a grain growth of the smallest α′ needles.

Fig. 5.a shows an orientation map taken in the side YZ plane of a stress-relieved cube. The picture's dimensions (75×50 μm) allowed to take a view of only a few prior β grains but the resolution (50 nm) allows to reach 95% of indexed pixels.
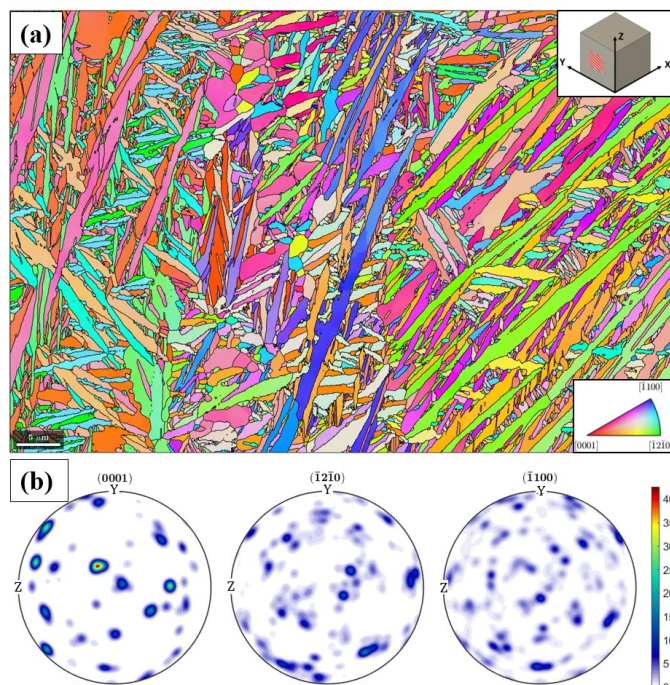
The α/α′ laths present a lot of morphological orientations within the prior β grains boundaries but the main inclination of the biggest laths is $\sim \pm 45°$ as it is also visible in Fig. 3. As a first approximation, the overall α/α′ texture appears random as the microstructure does not present laths colonies, this feature being inherited from the martensitic transformation. In contrast, the examination of the contour pole figure of the (0001) basal plane in Fig. 5.b reveal the presence of a few poles with a strong crystallographic texture. This could be explained by the variant selection phenomenon occurring during the β → α transformation of titanium alloys [26]. From each prior β grain, it is possible to generate 12 theoretical crystallographic orientations for the α phase, known as variants. In practice, a variant selection occurred during the β → α transformation and only some of the possible α′ orientations are inherited from one parent β grain and some preferred α′ crystallographic orientations are identifiable in Fig. 5 with respect to the variant selection phenomena. Otherwise, if one examines the crystallographic orientation at larger scales, including a high number of prior β grains, the α texture appears to be weak because of the high number of variants that are generated from different prior β grain orientations [27].

3.4. Impact and tensile properties

Tensile properties of the as-built and stress-relieved samples fabricated in the three studied orientations are listed in table 4. The results are the mean values from three tensile bars tested and the values in brackets are the relative standard deviation defined as the ratio of the standard deviation to the mean.

A major feature of these results is the low resistance measured in the as-built conditions and the enhancement observed after the stress-relieve treatment. As it was shown before, the microstructure is coarsened after the treatment which would normally lead to a drop in resistance, as shown in several other studies [5,8,18]. As the tensile tests in the mentioned studies are conducted with samples machined from L-PBF coupons, it is possible that the high tensile RS near the surface don't interfere with the extrinsic mechanical properties leading to higher levels of resistance. To confirm this scenario, further investigations are required: a possibility would be for instance to conduct tensile tests with samples machined into the block from the as-built fabrication.

Fig. 5. EBSD analyses on the YZ plane of a stress-relieved TA6V cube: orientation map of the α phase (a); corresponding (0001), ($\bar{1}2\bar{1}0$) and ($\bar{1}100$) contour pole figures (b). The building direction Z is the reference direction.

Table 4. Tensile properties of the as-built and stress-relieved samples.

Direction	$σ_Y$ (MPa)	UTS (MPa)	$ε_{fracture}$ (%)
Tensile properties of L-PBF TA6V in the as-built condition			
XY / YX	926 (1.0 %)	1070 (0.5 %)	4.8 (31.7 %)
XZ / YZ	897 (1.1 %)	1066 (0.3 %)	2.8 (64.8 %)
ZX / ZY	908 (1.5 %)	1075 (1.0 %)	4.2 (13.5 %)
Tensile properties of L-PBF TA6V in the stress-relieved condition			
XY / YX	1057 (0.8 %)	1138 (0.8 %)	4.6 (14.8 %)
XZ / YZ	1062 (0.8 %)	1151 (0.5 %)	3.2 (23.9 %)
ZX / ZY	1076 (1.4 %)	1156 (0.7 %)	8.8 (8.5 %)

The dispersions in the yield stresses (σ_Y) and ultimate tensile stresses (UTS) in both conditions are low for each orientation. In contrast, the dispersions of the elongations at break ($\varepsilon_{fracture}$) can exceed 50%, illustrating the effects of the raw surface state on the fracture behavior, with sharp corners and notches acting as stress concentrators [20, 24]. Only the elongation of the vertical orientation increases significantly after the heat treatment. Further investigations should also be conducted to depict a possible microstructural effect.

Impact properties measured on 10 as-built and 10 stress-relieved samples are displayed in table 5. It can be established that the absorbed energy (E_b) is nearly doubled after the heat treatment. A possible justification is the presence of the β_t phase which tends to increase the length of the crack propagation path (CPP). The theoretical value for a perfectly linear crack starting from the V-notch is 8 mm. The CPP was measured by extracting the path with ImageJ after revealing the crack by cutting and polishing a tested impact sample.

Table 5. Impact properties of the as-built and stress-relieved samples.

	As-built	Stress-relieved
E_b (J)	4.77 ± 0.14	10.34 ± 0.50
CPP length (mm)	11.32	12.18

4. Conclusion

The surface roughness, residual stresses, microstructure, texture and mechanical properties of TA6V L-PBF samples with raw surface state were investigated. The following conclusions are drawn from this work:

- The as-built microstructure obtained is 100% martensitic, with a hierarchical structure of the α' needles and a weak texture. High tensile RS are measured near the surface with the hypothesis of a possible impact on the resistance properties. The surface roughness affects the ductility.
- The stress-relieve heat treatment eliminates the majority of the RS and prevent cracks and deformation of the parts. The microstructure is composed of a mixture of α/α' with 2.7% of β_t. The ductility and the impact properties in the vertical direction were doubled but higher temperature treatments are necessary to meet the product requirements.

References

[1] Debroy T. et al. Additive manufacturing of metallic components – process, structure and properties. Progress in Materials Sci. 92; 2018. p. 112-224.
[2] Kong CJ. et al. High density Ti6Al4V via SLM processing: microstructure and mecha. properties. Solid freeform fab. symposium; 2011. p. 475-483.
[3] Poncelet O. et al. Critical assessment of the impact of process parameters on vertical roughness and hardness of thin walls of AlSi10Mg processed by L-PBF. Additive Manufacturing 38; 2021. 101801.
[4] Xu W. et al. Additive manufacturing of strong and ductile Ti-6Al-4V by selective laser melting via in situ martensite decomposition. Acta Materialia 85; 2015. p. 74-84.
[5] Cao S. et al. Role of martensite decomposition in tensile properties of SLMed Ti-6Al-4V. Journal of Alloys and Comp. 744; 2018. p. 357-363.
[6] Yang J. et al. Formation and control of martensite in Ti-6Al-4V alloy produced by SLM. Materials and Design 108; 2016. p. 308-318.
[7] Castioni F. et al. Plastic behavior of the α' phase in Ti-6Al-4V alloys. Materials Letters 283; 2021. 128719.
[8] Simonelli M. et al. Effect of the build orientation on the mechanical properties and fracture modes of SLM Ti-6Al-4V. Materials Science and Engineering A 616; 2014. p. 1-11.
[9] Mercelis P., Kruth JP. Residual stresses in selective laser sintering and selective laser melting. Rapid prototyping journal 12:5; 2006. p. 254-265.
[10] Khadar Syed. et al. An exp. study of residual stress and direction-dependence of fatigue crack growth behaviour in as-built and stress-relieved SLMed Ti6Al4V. Materials Sci. & Eng. A 755; 2019. p. 246-257.
[11] Ahmad B. et al. Residual stress evaluation in additively manufactured titanium (Ti-6Al-4V) and inconel 718 using the contour method and numerical simulation. Additive Manufacturing 22; 2018. p. 571-582.
[12] Anderson LS. et al. Investigating the residual stress distribution in selective laser melting produced Ti-6Al-4V using neutron diffraction. Materials Research Proceedings 4; 2018. p. 73-78.
[13] Knowles CR. et al. Residual stress measurements and structural integrity implications for selective laser melted Ti-6Al-4V. South African Journal of Industrial Engineering 23:2; 2012. p. 119-129.
[14] Vrancken B. et al. Res. stress via the contour method in compact tension specimens produced via SLM. Scripta Materialia 87; 2014. p. 29-32.
[15] Kasperovich G., Hausmann J. Improvement of fatigue resistance and ductility of Ti6Al4V processed by selective laser melting. Journal of Materials Processing Technology 220; 2015. p. 202-214.
[16] Leuders S. et al. On the mechanical behaviour of titanium alloy Ti6Al4V manufactured by selective laser melting: fatigue resistance and crack growth performance. International Journal of Fatigue 48; 2013. p. 300-307.
[17] Vilaro T. et al. As-fabricated and heat-treated microstructures of the Ti-6Al-4V alloy processed by selective laser melting. Metallurgical and Materials Transactions A 42; 2011. p. 3190-3199.
[18] Vrancken B. et al. Heat treatment of Ti6Al4V produced by Selective Laser Melting: microstructure and mechanical properties. Journal of Alloys and Compounds 541; 2012. p. 177-185.
[19] Kumar P. et al. Micro-and meso-structures and their influence on mechanical properties of selectively laser melted Ti-6Al-4V. Acta Materialia 154; 2018. p. 246-260.
[20] Tao P. et al. Tensile behavior of Ti-6Al-4V alloy fabricated by selective laser melting: effects of microstructures and as-built surface quality. China Foundry 15:4; 2018. p. 243-252.
[21] Yan X. et al. Effect of heat treatment on the phase transformation and mechanical properties of Ti6Al4V fabricated by selective laser melting. Journal of Alloys and Compounds 764; 2018. p. 1056-1071.
[22] Bélot JM. Fabrication additive métallique: les acteurs. Parachèvements, finitions, traitements thermiques et de surface. Conference: A3TS Post additive manufacturing; 2015.
[23] Fitzpatrick ME. Et al. Determination of residual stresses by X-Ray diffraction. Measurement Good Practice Guide 52:2; 2005.
[24] Liu S., Shin Y.C. Additive manufacturing of Ti6Al4V alloy: a review. Materials and Design 164; 2019. p. 107552.
[25] Ter Haar G.M., Becker T.H. Selective laser melting produced Ti-6Al-4V: post-process heat treatments to achieve superior tensile properties. Materials 11:1; 2018. p. 146.
[26] Burgers WG. On the process of transition of the cubic-body-centered modification into the hexagonal-close-packed modification of zirconium. Physica 1:7-12; 1934. p. 561-586.
[27] Simonelli M. et al. On the texture formation of selective laser melted Ti6Al4V. Metallur. and Materials Transactions A 45; 2014. p. 2863-2872